Biophysical Chemistry 170 (2012) 9–16

Contents lists available at SciVerse ScienceDirect

Biophysical Chemistry

journal homepage: http://www.elsevier.com/locate/biophyschem

Molecular dynamics simulation of HIV-1 fusion domain-membrane complexes: Insight into the N-terminal gp41 fusion mechanism

Siriporn Promsri [a], G. Matthias Ullmann [c], Supot Hannongbua [a,b,*]

[a] Computational Chemistry Unit Cell, Department of Chemistry, Faculty of Science, Chulalongkorn University, Bangkok 10330, Thailand
[b] Center of Excellence for Petroleum, Petrochemicals, and Advanced Materials, Chulalongkorn University, Bangkok 10330, Thailand
[c] Computational Biochemistry Group, Faculty of Biology, Chemistry and Geosciences, University of Bayreuth, 95447 Bayreuth, Germany

HIGHLIGHTS

- The conformations of the membrane-bound the HIV gp41 fusion peptides were examined.
- Inclusion of residues 17–23 was found to play important role in the fusion ability.
- A mixture of helical and β-strand structures was found to be a membrane-bound state.
- The peptide does affect the structural and dynamical characteristics of the lipids.
- The fusion ability depends on the alignment of fusion peptide structure.

GRAPHICAL ABSTRACT

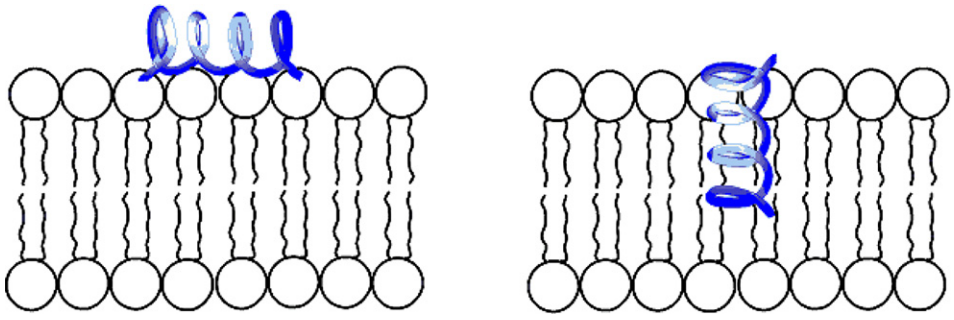

ARTICLE INFO

Article history:
Received 29 November 2010
Received in revised form 24 June 2012
Accepted 9 July 2012
Available online 16 July 2012

Keywords:
Fusion peptide
HIV-1 gp41
Membrane fusion
Molecular dynamics simulation
DMPC
Order parameter

ABSTRACT

To understand how viral proteins fuse with the cell membrane, a process that is important for the initial stages of infection, the conformation of the membrane-bound viral fusion peptides (FPs) must be identified. Here, molecular dynamics (MD) simulations were performed to investigate the conformation of the FP-16 and FP-23 of human immunodeficiency virus (HIV) bound to a dimyristoyl phosphatidylcholine (DMPC) bilayer. All FPs were found to penetrate into the bilayer despite the different initial orientations. In addition, the inclusion of residues 17 to 23 was found to play significant role in the fusion ability. Each of the FPs adopts at least two distinct conformations (predominantly α-helical and β-structures) while association with membrane. The peptide seriously affects structural and dynamical parameter of the contacted lipids. The previously experimental data together with our simulation data reveal that fusion ability depends on the membrane-associated conformation and alignment of the peptide.

1. Introduction

Infection of a target cell by enveloped viruses, such as human immunodeficiency virus type 1 (HIV-1) and influenza virus, requires fusion between the viral envelope and host cell membrane [1]. The fusion event is mediated by anchoring of the fusion protein on the cell membrane surface via the fusion peptide (FP) domain which usually located at the N-terminus in many viruses. In the case of HIV, the envelope glycoproteins are typically homotrimers in which each monomer is proteolytically cleaved to generate two subunits, gp120 and gp41, the latter of which is responsible for the membrane fusion process [2–4]. The N-terminal gp41-FP is highly conserved with corresponding domains of other enveloped virus, and its first 16 residues are mostly hydrophobic followed by another seven moderately polar residues.

* Corresponding author at: Department of Chemistry, Faculty of Science, Chulalongkorn University, Phyathai Road, Patumwan, Bangkok, 10330, Thailand. Tel.: +66 2 218 7602; fax: +66 2 218 7603.
E-mail address: supot.h@chula.ac.th (S. Hannongbua).

0301-4622/$ – see front matter © 2012 Elsevier B.V. All rights reserved.
doi:10.1016/j.bpc.2012.07.002

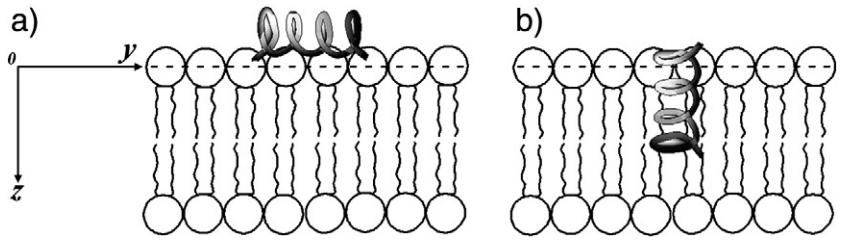

Fig. 1. Schematic diagram showing the initial FP-membrane structure in two different FP configurations with respect to the bilayer surface showing the helical axis of FP at (a) 0° and (b) 90° to the phospholipid horizontal plane. The FP is shown as a ribbon structure. Dashed line indicates the center of the water–lipid interface (at the horizontal line $y=0$).

There have been many efforts to determine the structure of the FPs and the mode of interaction with the membrane from a variety of experimental method (NMR, FTIR, CD, ESR) [5–22] as well as molecular dynamics (MD) simulations [7,19,23–33]. The three-dimensional structure has been widely studied in membrane-mimicking environment to learn more about the fusion mechanism. However, the mechanism by which the N-terminal FPs promote fusion is not clear, although the literature does offer several suggestions. Several authors have suggested that some peptide secondary structures (α-helical or β-stranded) are fusogenic whilst others are not [34–37]. Other authors have suggested that FPs perturb the bilayer surface [38,39], and in addition, changes in the order parameters of the lipid acyl chains has been reported in the presence of the FP [29,40].

In this study, molecular dynamics (MD) simulations for the gp41 N-terminal FP in a dimyristoyl phosphatidylcholine (DMPC) bilayer were performed. Each of the 16- and 23-residue FPs , designated here as FP-16 and FP-23 respectively, were examined in two different states of the N- and C-terminus (charged and neutral) and with two different orientations with respect to the bilayer surface (0° and 90°), as shown in Fig. 1. The sequences of the peptides and their designations are given in Table 1. The explicit MD simulations were able to determine the membrane structures of these FPs, which are consistent with the currently available experimental determinations, and also provide insight into the secondary structure of the FPs and the bilayer perturbation upon the binding of these active FPs to the bilayer.

2. Computational details

2.1. Fusion peptide (FP)

The initial conformation of the N-terminal gp41 FP was obtained from NMR spectroscopic analysis [10]. The models from a protein data bank file, which is helical between Ile-4 and Gly-20, were extracted. The FP-16 and FP-23 in two different states of the N- and C-terminus (charged and neutral states) and two different orientations with respect to the bilayer surface (0° and 90°) were generated. The sequences of the peptides and their designations are given in Table 1.

2.2. Initial structures

The initial structures of the peptide-bilayer system were constructed using the CHARMM program [41] in which the procedure

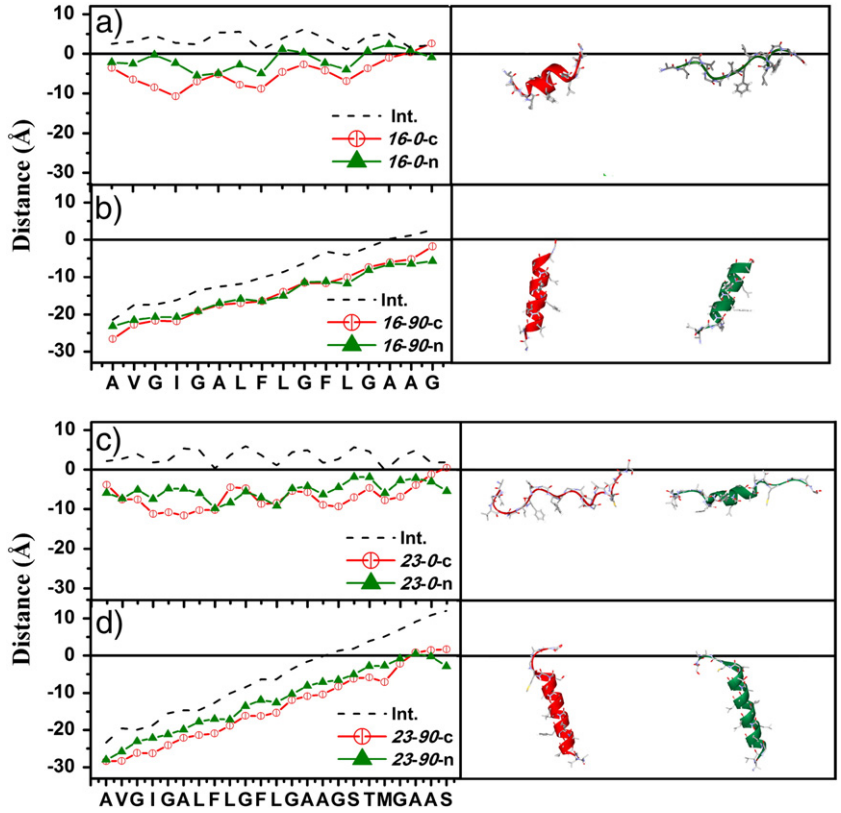

Fig. 2. Insertion depth of the residues of the FP in the DMPC membrane. The distance between the Cα atoms of FP and the center of the water-lipid interface was calculated as a mean z coordinate of the phosphorus atoms. Ribbon representative structures of the FPs in charged and neutral terminus are also shown in red and green, respectively.

developed by Woolf and Roux [42–45] was applied. To prepare the initial structures for the simulations, the area per lipid was taken from experimental value of 59.8 Å^2 at 30 °C. The cross-sectional area of the FP-16 and FP-23 was calculated to be 380.7 Å^2 and 489.9 Å^2, respectively. Therefore, the layer containing the above mentioned FPs should then contain six and eight lipids less than the FP-free layer. The 128 DMPC molecules were selected randomly from the 2000 pre-equilibrated DMPC structures taken from the data of Roux. To equalize the area of the top and bottom leaflets, 61 and 60 DMPC molecules were placed in the FP-containing layer whereas 67 and 68 DMPC molecules were placed in the FP-free layer for the FP-16 and FP-23 systems, respectively. The initial size of the simulation box was determined by the cross-sectional area of the FP, the number of DMPC molecules and the number of water molecules of the bilayer. The FP was initially placed in the upper leaflet of the bilayer keeping the helical axis at either 0° or 90° with respect to the bilayer surface, as shown schematically in Fig. 1. For the helical axis at 90°, the Gly-16 of all FPs was positioned at the bilayer surface. The systems were then fully hydrated by overlaying a pre-equilibrated water box of the appropriate dimensions in the *x* and *y* directions (see Fig. 1).

2.3. Initial simulations

The minimization was first carried out with the CHARMM program [41] using the all-atom force field and TIP3 [46] water model. To speed up the simulations using the GROMACS program package [47], the option was switched to united-atom force fields. The forced fields for lipids and peptides were taken from Tieleman [48] and GROMACS, respectively. The SPC model [49] was used for water molecules. The systems were coupled to a heat bath of 303 K. Position restrained simulations of each FP were performed for 2 ns to equilibrate the membrane structure. A number of position constraints were used at the beginning of the ensuing equilibration period to ensure a smooth relaxation of the system towards an equilibrated configuration.

2.4. NPT simulations

Starting configurations were obtained by the position-restrained simulation at 2 ns. The MD simulations were performed employing an NPT ensemble (*i.e.*, constant number of particles, pressure, and temperature) for the eight systems summarized in Table 1 using the GROMACS program package [47]. The simulations The LINCS algorithm [50] was used to constrain all bond lengths of the lipid molecules, whereas the SETTLE algorithm [51] was used for water molecules. Periodic boundary conditions were applied in all three dimensions. The time step in all simulations was set to 2 fs. The energies and trajectories were stored every 1 and 10 ps, respectively, and the temperature was kept at 303 K. The pressure coupling was scaled to 1 bar with a time constant of 0.5 ps and applied semi-isotropically; the pressure along the *xy* coordinate and *z* coordinate defined in Fig. 1 were allowed to vary independently. All simulations were performed for 100 ns.

2.5. Control simulation

For the control simulation, the 128 DMPC molecules were examined and each leaflet had 64 DMPC molecules. The same steps as above were performed apart from the position restrained simulations. A total of 100 ns of MD simulations were performed and then used for the subsequent analysis.

3. Results and discussion

3.1. Depth of insertion

To monitor how deep the peptides insert into the bilayer, the location of each residue of the FPs was measured in terms of the distance of each residue with respect to the bilayer normal. Fig. 2 shows the insertion depth of a given residue which corresponds to the average distance between its Cα atom and the center of the water-membrane interface, defined as a mean *z* coordinate of the phosphorus atom (see Fig. 1 for axes definition). The resulting distribution plots for the FP-16 and FP-23 systems are shown in Fig. 2. The horizontal line at $y = 0$ indicates the interface between the water and the membrane, whereas the initial position of the FPs for each system is represented by the dashed line. For simplicity, the *l*-*a*-c/n notation is used where *l*, *a*, c/n denote the length (***l*** = 16 or 23 amino acid residues), the insertion angle ($a = 0$ or 90°) and the types of N- and C-terminus (either charged (**c**) or neutral (n)) of the FPs (see Table 1).

It can be seen that all FPs penetrate into the bilayer despite their different initial orientations. Detailed characteristics of the binding are presented in Fig. 2. The effect of charged termini can be clearly seen for both insertion angle ($a = 0°$ and 90°) where the charged zwitterionic peptide was inserted deeper into the bilayer than the neutral one. The only exception is in the case of FP-16 when $a = 90°$ (Fig. 2b), where no difference was found in terms of the insertion depth of the *16-90*-c and *16-90*-n peptide.

Considering the effect of the FP length, all the FPs of the FP-23 systems were observed to penetrate deeper into the lipid bilayer than the FP-16 systems relative to their initial positions (Fig. 2). The maximal penetration depth (~17 Å) is observed for residue Ala-6 of *23-0*-c system (Fig. 2c). Therefore, the inclusion of the residues 17 to 23 to the FPs was found to play a significant role in their fusion. This is especially true for the neutral peptides with $a = 0°$, *i.e.* the *23-0*-n, which penetrated much deeper than the corresponding *16-0*-n. In addition, in the case of FP-23 when $a = 90°$ (Fig. 2d), the *23-90*-c was found to fuse deeper into the bilayer, relative to the charged *16-90*-n. However, there is no significant difference of the peptides with neutral terminus, i.e. the *16-90*-n and *23-90*-n in term of the insertion depth.

3.2. Secondary structure

To examine the theoretical secondary structure of the FPs, the DSSP [52] program was employed using the *do_dssp* utility command from the GROMACS [47] package to investigate the time evolutions of

Table 1
Amino acid sequences of the fusion peptides (FPs) and the notation used in the manuscript hereafter.

Notation	No. of residues[a]	Angle of insertion[b]	Type of N- and C-terminus	Amino acid sequence
16-0-c	16	0°	Charged	NH_3^+– A V G I G A L F L G F L G A A G –COO^-
16-0-n	16	0°	Neutral	NH_2– A V G I G A L F L G F L G A A G –COOH
16-90-c	16	90°	Charged	NH_3^+– A V G I G A L F L G F L G A A G –COO^-
16-90-n	16	90°	Neutral	NH_2– A V G I G A L F L G F L G A A G –COOH
23-0-c	23	0°	Charged	NH_3^+- A V G I G A L F L G F L G A A G S T M G A R S –COO^-
23-0-n	23	0°	Neutral	NH_2– A V G I G A L F L G F L G A A G S T M G A R S –COOH
23-90-c	23	90°	Charged	NH_3^+- A V G I G A L F L G F L G A A G S T M G A R S –COO^-
23-90-n	23	90°	Neutral	NH_2– A V G I G A L F L G F L G A A G S T M G A R S –COOH

[a] The number of amino acid residues in the FP sequence.
[b] The angle of fusion between the helical axis of the FP and the horizontal plane of the phospholipid bilayer.

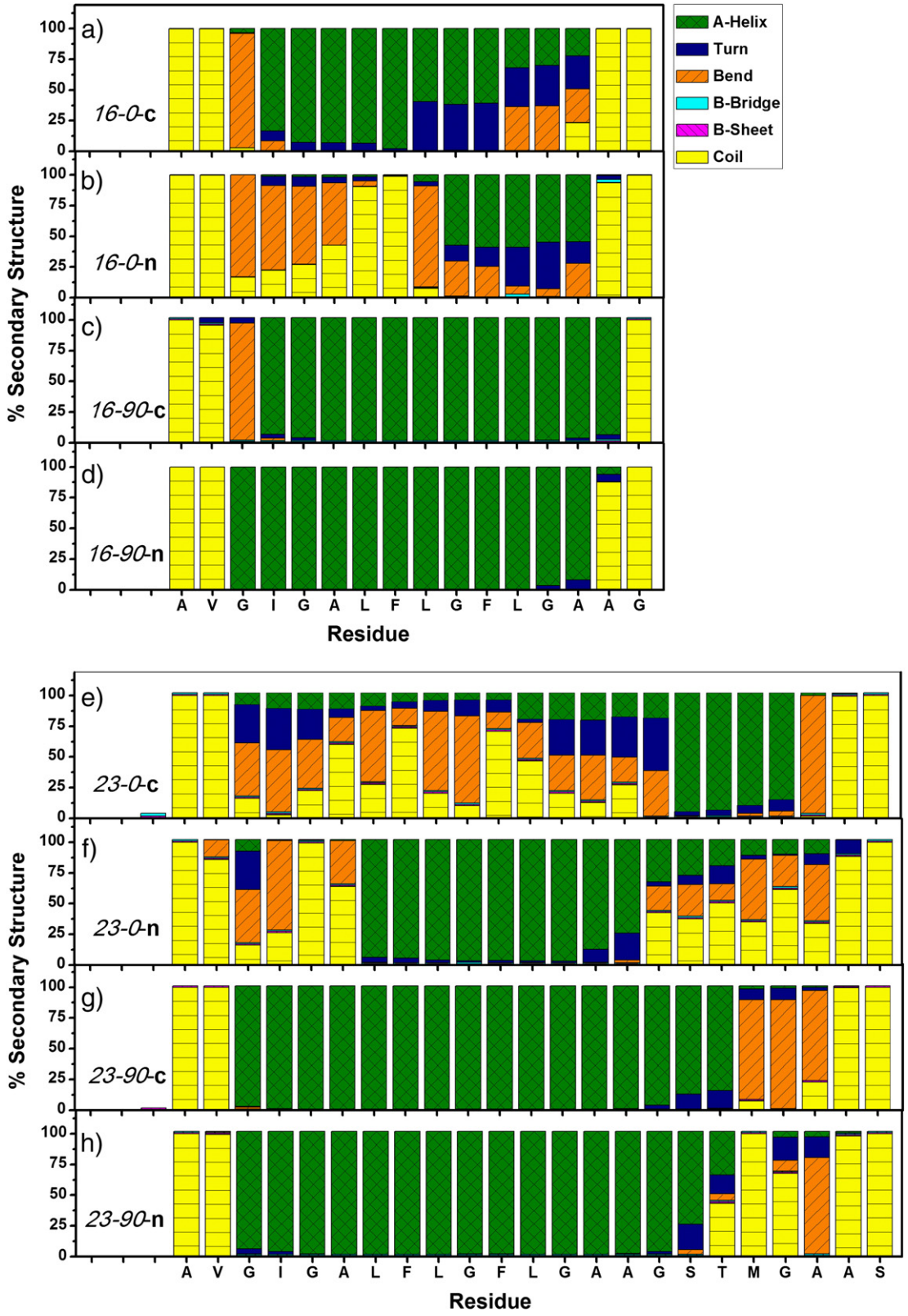

Fig. 3. Secondary structure of the N-terminal gp41 FPs. The relative occurrence of each of the FP residues in different secondary structure elements, as obtained during the entire 100 ns MD simulations of the FP in the presence of DMPC. Green and yellow show α-helical and coiled structures, respectively.

the secondary structure of the membrane-bound FP-16 and FP-23. The plots of the %structure of all FPs are shown in Fig. 3.

The secondary structure map of the FPs computed as a function of the simulation time exhibits various conformations. The plots of the %structure of all FPs show that very different types of secondary structures emerge upon interaction with the lipid (Fig. 3.). The FPs adopt predominantly α-helical and β-strand conformations. In addition, the structures of the N- and C-terminal tails are highly flexible and

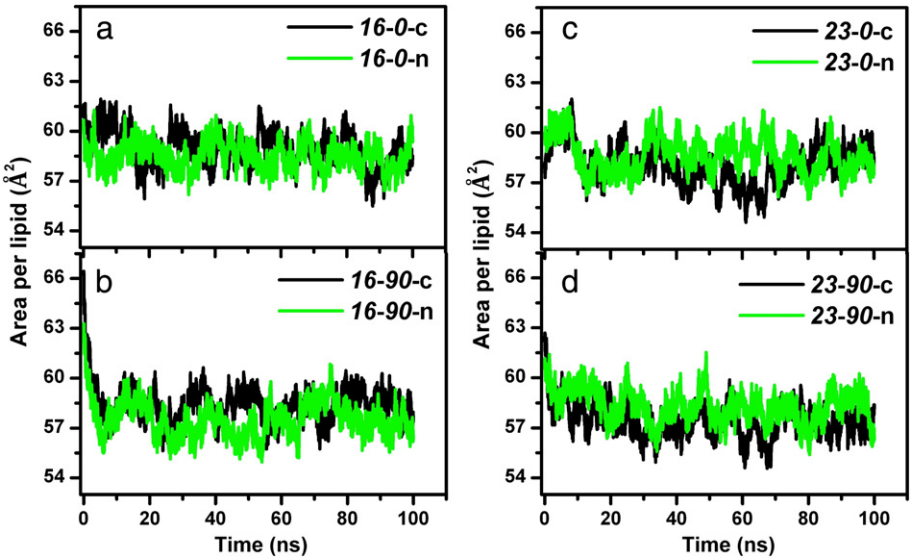

Fig. 4. The time evolution of the area per lipid for the (a, b) 16-residue and (c, d) 23-residue FP-membrane complexes with an initial helical axis of (a, c) 0° and (b, d) 90° with respect to the bilayer surface.

more or less unstructured or coiled. Considering the FPs when $a = 0°$, it is seen that the peptides partly lose their initial α-helical structure and adopt other conformations. It clearly shows that the presence of water-membrane interface significantly destabilizes α-helical conformation of the peptide. This is due to the prominent amphiphilic character of the helix which a number of apolar side chains are exposed to a highly water environment. In the result, the helix structure of the FPs tends to distort and shield the hydrophobic side chains from water. This indicates that the instability of the α-helical conformation on membrane surface can be induced by strong contacts of the peptide with the water-lipid interface. However, this is different when the initial structure of the FPs was perpendicular to the membrane surface, as here the α-helical structure was observed throughout the simulation (Fig. 3). Clearly, the hydrophobic core membrane stabilizes the α-helical structure of the FPs. Such systems reveal the domination of hydrophobic-hydrophobic contacts, which reflects the correspondence between a highly hydrophobic fusion domain and the hydrophobic interior of the membrane.

There is consistency between our results and earlier experimental work [17] with reports of a mixture of helical and β-strand conformations of the FPs while association with membrane. Taking this experimental data together with our simulation data reveals that FP

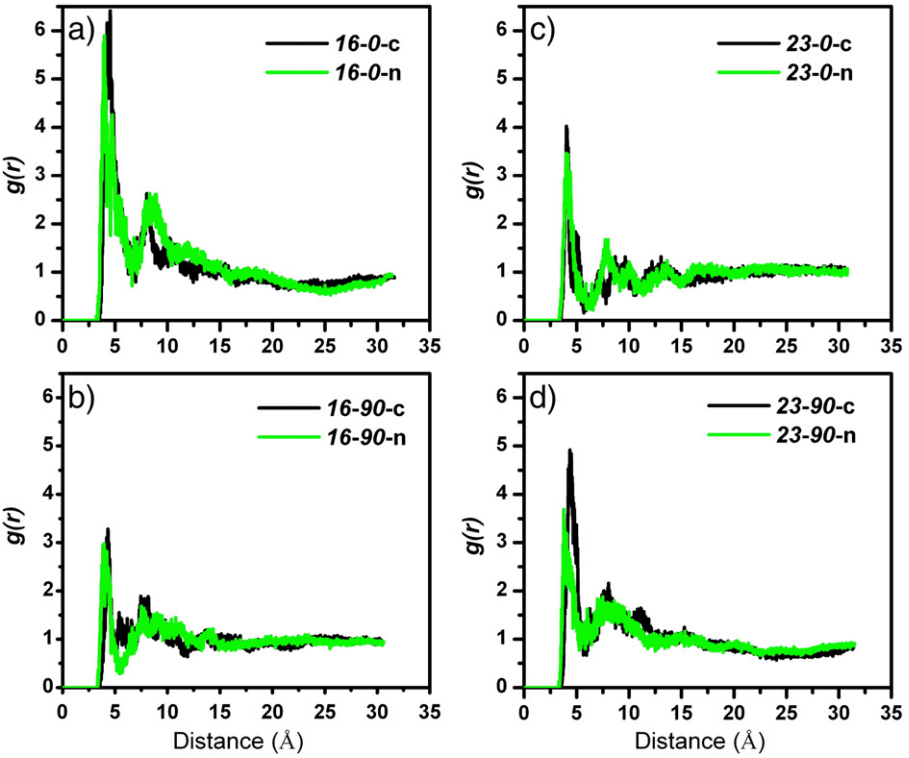

Fig. 5. Radial distribution functions (g(r)) centred at the centre of mass of the FP to the phosphorus in the headgroup region of the bilayer for (a, b) the 16-residue FP and (c, d) the 23-residue FP-membrane complexes with an initial helical axis of (a, c) 0° and (b, d) 90° with respect to the bilayer surface.

insertion into the lipid bilayer depends on the membrane-associated conformation and alignment of the peptide. Furthermore, fusion activity of the FPs might not correlate with the type secondary structure (α-helix, β-sheet, or mixed). It is also possible that there is a transient fusogenic structure that is flexible or unstructured rather than a well-structured α-helical or β-strand conformation.

3.3. Area per lipid

One of the most fundamental characteristics of the lipid bilayer is the average area per lipid. Although a wide range of these values have been obtained from model membranes via experiments [53,54], it is also very useful as a means of monitoring the equilibrium process from a computational point of view. Fig. 4 shows the area per lipid (DMPC) for all simulations as a function of time, where the average area per lipid for all systems is in the range of 57.4–59.0 Å^2. This range is just slightly lower than the previously reported experimentally determined value of 59.8 ± 1.9 Å^2 (at 30 °C) [54]. The reliability of the simulation results is thus supported to some extent by this consistency.

3.4. Radial distribution functions

To characterize the structure of the peptide-membrane complex in more detail, radial distribution functions (RDFs), which describe how the atomic density varies as a function of the distance from one particular atom, from the center of mass of the FP to the phosphorus atom in the headgroup of the lipid bilayer were computed. The results are shown in Fig. 5. The plots for all systems show the first maxima of ~4.8 Å followed by the first minima of ~6 Å. This number indicates that first shell of the headgroup of the lipid lies within the radius of 6 Å. This radius was then used to examine the changes in the membrane character due to the presence of the FP. That is the

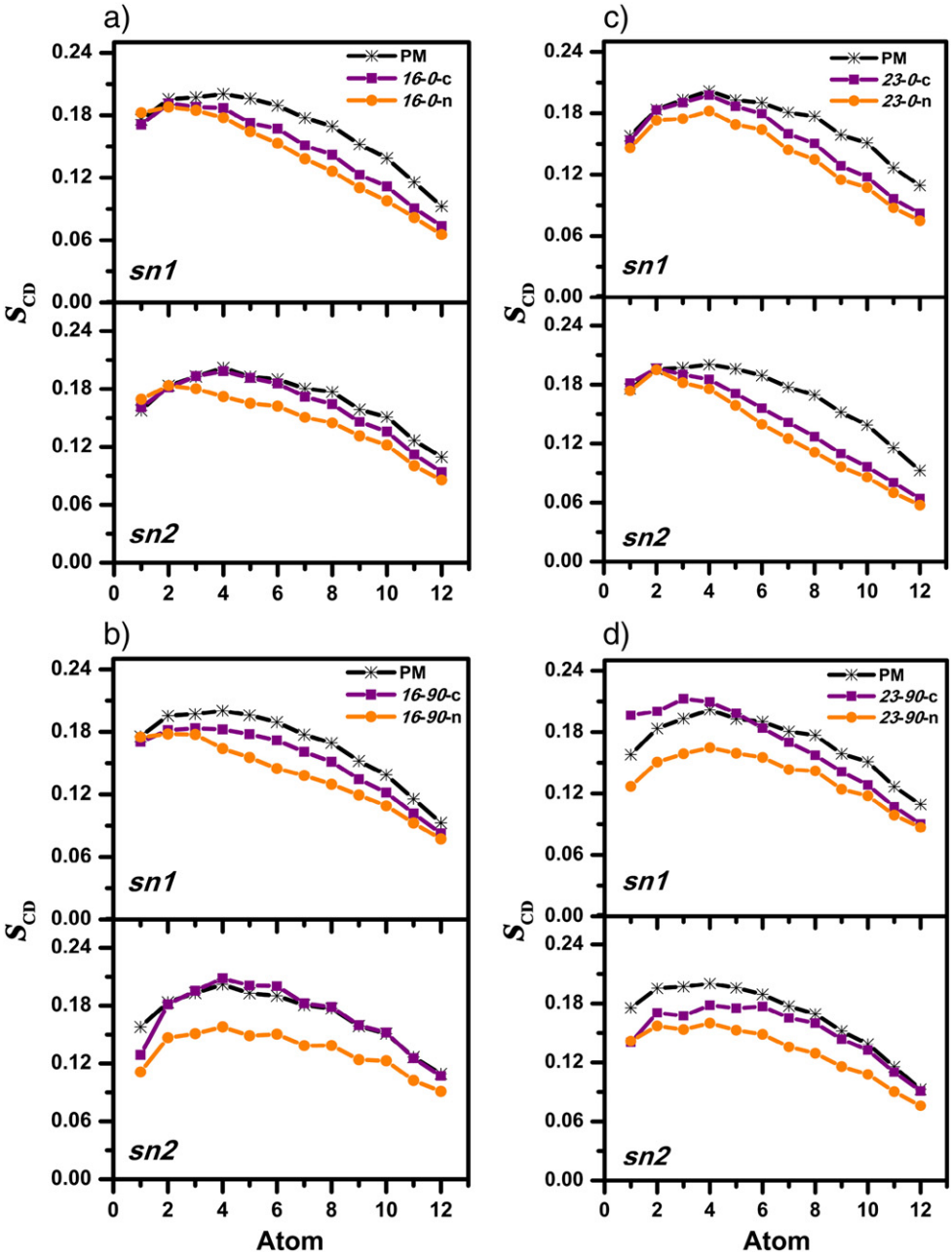

Fig. 6. Average order parameter (S_{CD}) values for the *sn*1 and *sn*2 acyl chains of the DMPC bilayer and its complexes with the (a, b) 16-residue FP- and (c, d) 23-residue FP-membrane complexes with an initial helical axis of (a, c) 0° and (b, d) 90° with respect to the bilayer surface. PM denotes the order parameter of the DMPC membrane without the FPs (black).

order parameter of the membrane within a 6 Å radius from the Cα of the FP was calculated for each system.

3.5. Ordering of lipid acyl chains

The ordering of the lipid acyl chain methylene segments can be characterized by the deuterium order parameter, S_{CD}, which can be measured by the NMR technique. The S_{CD} may be defined for every methylene group in the chain as:

$$S_{CD} = \left\langle 3/2\ \cos^2\theta - 1/2 \right\rangle$$

where θ is the angle between the CD-bond (for experimental determination) or CH-bond (for simulations) and the normal bilayer, whilst the brackets denote an average over time over all of the lipids (or over a subset of the membrane lipids). The value of S_{CD} quantifies the degree of reorientation that occurs on the NMR time scale. In a united-atom simulation, one can reconstruct the CH-bond at their equilibrium positions on the basis of the backbone chain configuration.

The calculated order parameter of the tails can be directly compared to that obtained from the NMR analysis of deuterated DMPC. Experimentally, the order parameter along the hydrocarbon chains of a fully hydrated DMPC bilayer is usually determined at 30 °C. A useful comparison parameter is the average of the CH order parameter in the plateau region. The order parameters were calculated separately for the two chains (*sn*1 and *sn*2) of the DMPC molecules for each system and were plotted against the position in the chain. The *sn*2 chain is attached to the middle carbon of the glycerol backbone and is therefore, on average, slightly closer to the membrane surface than the *sn*1 chain.

Because the FP does not span across the entire membrane from one side to the other side, its effect on the order parameter of the contacted lipids has to be studied separately. Fig. 6 shows the results from the theoretical (MD simulations) analysis for both the *sn*1 and *sn*2 acyl chain order parameters for DMPC in the FP-membrane model, and the protein-free lipid control, within a radius of 6 Å from the center of mass of the FP (as mentioned above). The orientational order parameter profiles for the acyl chains in the absence of the peptide are typical of liquid crystalline DMPC bilayers but are slightly lower than the experimentally obtained values (data not shown). Note that the S_{CD} is ~0.20 close to the glycerol group, and tends towards zero toward the end of the tail. The acyl chains are therefore reasonably ordered close to the headgroup.

The results show that binding of the FP considerably destabilizes hydrocarbon tail of the lipid. This is reflected in the decrease of S_{CD} values both of the *sn*1 and *sn*2 as shown in Fig. 6. The effect of neutral termini can be clearly seen for all systems where the S_{CD} of the neutral FP-membrane system is lower than the charged FP-membrane and the peptide-free lipid systems. This indicated that the neutral termini can induce the disordering of the acyl chain of the lipid more than the charged one.

Note that the effect on the ordering of the acyl chains was significantly different for the different FPs, although they all induced the disordering of the acyl chain in terms of a significant reduction in the S_{CD} values. This is due to the position of the FPs in the bilayer along the normal bilayer. The lipids closest to the peptide show a significant reduction in their S_{CD} values, compared to in a pure bilayer. In accord, a qualitatively similar reduction in the order parameter near the embedded peptides was observed in the simulation of alamethicin, influenza M2 and OmpF embedded in a POPE membrane [55].

4. Conclusions

In the present study, the results of MD simulations of the FP-16 and FP-23 of HIV gp41 with a DMPC bilayer are presented. The simulations showed that both FPs in both orientations insert into the bilayer notwithstanding their different initial orientations. The zwitterionic charged FPs, when starting from the parallel configuration, inserts deeper into the bilayer than the theoretical neutral peptide does. The analysis of the secondary structure indicated that the FPs adopt both α-helical and β-strand conformations during the simulation time. This is consistent with the experimental data [17] that a mixture of helical and β-strand conformations of the FPs is a structure for membrane-bound states. Taking the published experimental data together with our simulation data here supports that fusion activity of the FPs might not correlate with the type of secondary structure (α-helix, β-sheet, or mixed).

The FP's effect on the lipid bilayer was demonstrated in terms of the order parameter. FPs induce some membrane disorder, but this is local being limited to those lipids in the vicinity of the peptide, in agreement with previous experimental results.

Finally, we should stress that the membrane fusion process is much more complex than the simplified systems used in this molecular modeling approach. There are too many factors that have to be properly taken into account to determine peptide–membrane interaction, *i.e.*, the conformation flexibility of the peptides, the tilt and orientation patterns, the effect of the membrane compositions, etc. Nevertheless, the present results provide information on the embedded peptide and the bilayer at the molecular level and are complementary with the experimental data.

Acknowledgements

Computing facilities were provided by the Computational Biochemistry group at Bayreuth University, Germany. This work was financially supported by the Thailand Research Fund (TRF) and the Deutscher Akademischer Austauschdienst (DAAD). We further thank the TRF (DPG5480002), the National Research University Project of Thailand, Office of the Higher Education Commission (HR1155A-55), and the Thai Government Stimulus Package 2 (TKK2555) under the Project for Establishment of Comprehensive Center for Innovative Food, Health Products and Agriculture. S.P. acknowledges a Royal Golden Jubilee Scholarship, Grant. No. PHD/0240/2546 and a DAAD Scholarship.

References

[1] R.M. Epand, Fusion peptides and the mechanism of viral fusion, Biochimica et Biophysica Acta 1614 (2003) 116–121.
[2] L.K. Tamm, J. Crane, V. Kiessling, Membrane fusion: a structural perspective on the interplay of lipids and proteins, Current Opinion in Structural Biology 13 (2003) 453–466.
[3] J. Torres, T.J. Stevens, M. Samso, Membrane proteins: the "Wild West" of structural biology, Trends in Biochemical Sciences 28 (2003) 137–144.
[4] R. Brasseur, T. Pillot, L. Lins, J. Vandekerckhove, M. Rosseneu, Peptides in membranes: tipping the balance of membrane stability, Trends in Biochemical Sciences 22 (1997) 167–171.
[5] W. Qiang, J. Yang, D.P. Weliky, Solid-state nuclear magnetic resonance measurements of HIV fusion peptide to lipid distances reveal the intimate contact of [beta] strand peptide with membranes and the proximity of the Ala-14–Gly-16 Region with Lipid Headgroups, Biochemistry 46 (2007) 4997–5008.
[6] C.M. Wasniewski, P.D. Parkanzky, M.L. Bodner, D.P. Weliky, Solid-state nuclear magnetic resonance studies of HIV and influenza fusion peptide orientations in membrane bilayers using stacked glass plate samples, Chemistry and Physics of Lipids 132 (2004) 89–100.
[7] B. Barz, T.C. Wong, I. Kosztin, Membrane curvature and surface area per lipid affect the conformation and oligomeric state of HIV-1 fusion peptide: a combined FTIR and MD simulation study, Biochimica et Biophysica Acta 1778 (2008) 945–953.
[8] X. Han, J.H. Bushweller, D.S. Cafiso, L.K. Tamm, Membrane structure and fusion-triggering conformational change of the fusion domain from influenza hemagglutinin, Nature Structural Biology 8 (2001) 715–720.
[9] T. Korte, R.F. Epand, R.M. Epand, R. Blumenthal, Role of the Glu residues of the influenza hemagglutinin fusion peptide in the pH dependence of fusion activity, Virology 289 (2001) 353–361.
[10] C.P. Jaroniec, J.D. Kaufman, S.J. Stahl, M. Viard, R. Blumenthal, P.T. Wingfield, A. Bax, Structure and dynamics of micelle-associated human immunodeficiency virus gp41 fusion domain, Biochemistry 44 (2005) 16167–16180.
[11] B. Bechinger, L.M. Gierasch, M. Montal, M. Zaloff, S.J. Opella, Orientations of helical peptides in membrane bilayers by solid-state NMR spectroscopy, Solid State Nuclear Magnetic Resonance Spectroscopy 7 (1996) 185–192.

[12] K.F. Morris, X. Gao, T.C. Wong, The interactions of the HIV gp41 fusion peptides with zwitterionic membrane mimics determined by NMR spectroscopy, Biochimica et Biophysica Acta 1667 (2004) 67–81.
[13] Z. Zhou, J.C. Macosko, D.W. Hughes, B.G. Sayer, J. Hawes, R.M. Epand, 15N NMR study of the ionization properties of the influenza virus fusion peptide in zwitterionic phospholipid dispersions, Biophysical Journal 78 (2000) 2418–2425.
[14] M.E. Haque, V. Koppaka, P.H. Axelsen, B.R. Lentz, Properties and structures of the influenza and HIV fusion peptides on lipid membranes: implications for a role in fusion, Biophysical Journal 89 (2005) 3183–3194.
[15] A. Saez-Crion, J.L. Nieva, Conformational transitions of membrane-bound HIV-1 fusion peptide, Biochim. Biophys. Acta - Biomembranes 1564 (2002) 57–65.
[16] J. Yang, M. Prorok, F.J. Castellino, D.P. Weliky, Oligomeric [beta]-structure of the membrane-bound HIV-1 fusion peptide formed from soluble monomers, Biophysical Journal 87 (2004) 1951–1963.
[17] W. Qiang, D.P. Weliky, HIV fusion peptide and its cross-linked oligomers: efficient syntheses, significance of the trimer in fusion activity, correlation of [beta] strand conformation with membrane cholesterol, and proximity to lipid headgroups, Biochemistry 48 (2009) 289–301.
[18] Y. Li, L.K. Tamm, Structure and plasticity of the human immunodeficiency virus gp41 fusion domain in lipid micelles and bilayers, Biophysical Journal 93 (2007) 876–885.
[19] D. Grasnick, U. Sternberg, E. Strandberg, P. Wadhwani, A. Ulrich, Irregular structure of the HIV fusion peptide in membranes demonstrated by solid-state NMR and MD simulations, European Biophysics Journal 40 (2011) 529–543.
[20] S. Afonin, U.H.N. Dürr, R.W. Glaser, A.S. Ulrich, 'Boomerang'-like insertion of a fusogenic peptide in a lipid membrane revealed by solid-state 19F NMR, Magnetic Resonance in Chemistry 42 (2004) 195–203.
[21] Z. Zheng, R. Yang, M.L. Bodner, D.P. Weliky, Conformational flexibility and strand arrangements of the membrane-associated HIV fusion peptide trimer probed by solid-state NMR spectroscopy, Biochemistry 45 (2006) 12960–12975.
[22] P. Wadhwani, J. Reichert, J. Bürck, A. Ulrich, Antimicrobial and cell-penetrating peptides induce lipid vesicle fusion by folding and aggregation, European Biophysics Journal 41 (2012) 177–187.
[23] P. Lagüe, B. Roux, R.W. Pastor, Molecular dynamics simulations of the influenza hemagglutinin fusion peptide in micelles and bilayers: conformational analysis of peptide and lipids, Journal of Molecular Biology 354 (2005) 1129–1141.
[24] A. Panahi, M. Feig, Conformational sampling of influenza fusion peptide in membrane bilayers as a function of termini and protonation states, The Journal of Physical Chemistry. B 114 (2009) 1407–1416.
[25] J. Li, P. Das, R. Zhou, Single mutation effects on conformational change and membrane deformation of influenza hemagglutinin fusion peptides, The Journal of Physical Chemistry. B 114 (2010) 8799–8806.
[26] Q. Huang, C.L. Chen, A. Herrmann, Bilayer conformation of fusion peptide of influenza virus hamgglutinin: a molecular dynamics study, Biophysical Journal 87 (2004) 14–22.
[27] V.K. Gangupomu, C.F. Abrams, All-atom models of the membrane-spanning domain of HIV-1 gp41 from metadynamics, Biophysical Journal 99 (2010) 3438–3444.
[28] D. Bechor, N. Ben-Tal, Implicit solvent model studies of the interactions of the influenza hemagglutinin fusion peptide with lipid bilayers, Biophysical Journal 80 (2001) 643–655.
[29] P.E. Volynsky, A.A. Polyansky, N.A. Simakov, A.S. Arseniev, R.G. Efremov, Effect of lipid composition on the "membrane response" induced by a fusion peptide, Biochemistry 44 (2005) 14626–14637.
[30] R.G. Efremov, D.E. Nolde, P.E. Volynsky, A.A. Chernyavsky, P.V. Dubovskii, A.S. Arseniev, Factors important for fusogenic activity of peptides: molecular modeling study of analogs of fusion peptide of influenza virus hemagglutinin, FEBS Letters 462 (1999) 205–210.
[31] T.C. Wong, Membrane structure of the human immunodeficiency virus gp41 fusion peptide by molecular dynamics simulation: II. The glycine mutants, Biochimica et Biophysica Acta, Biomembranes 1609 (2003) 45–54.
[32] S. Kamath, T.C. Wong, Membrane structure of the human immunodeficiency virus gp41 fusion domain by molecular dynamics simulation, Biophysical Journal 83 (2002) 135–143.
[33] M.W. Maddox, M.L. Longo, Conformational partitioning of the fusion peptide of HIV-1 gp41 and its structural analogs in bilayer membranes, Biophysical Journal 83 (2002) 3088–3096.
[34] C. Gray, S.A. Tatulian, S.A. Wharton, L.K. Tamm, Effect of the N-terminal glycine on the secondary structure, orientation, and interaction of the influenza hemagglutinin fusion peptide with lipid bilayers, Biophysical Journal 70 (1996) 2275–2286.
[35] J.L. Nieva, S. Nir, A. Muga, F.M. Goni, J. Wilschut, Interaction of the HIV-1 fusion peptide with phospholipid vesicles: different structural requirements for fusion and leakage, Biochemistry 33 (1994) 3201–3209.
[36] T. Matsumoto, Membrane destabilizing activity of influenza virus hemagglutinin-based synthetic peptide: implications of critical glycine residue in fusion peptide, Biophysical Chemistry 79 (1999) 153–162.
[37] E.I. Pecheur, I. Martin, A. Bienvene, J.M. Ruysschaert, D. Hoekstra, Protein-induced fusion can be modulated by target membrane lipids through a structural switch at the level of the fusion peptide, The Journal of Biological Chemistry 275 (2000) 3936–3942.
[38] C. Curtain, F. Separovic, K. Nielsen, D. Craik, Y. Zhong, A. Kirkpatrick, The interactions of the N-terminal fusogenic peptide of HIV-1 gp41 with neutral phospholipids, European Biophysics Journal 28 (1999) 427–436.
[39] R.M. Epand, R.F. Epand, Relationship between the infectivity of influenza virus and the ability of its fusion peptide to perturb bilayers, Biochemical and Biophysical Research Communications 202 (1994) 1420–1425.
[40] X. Han, D.A. Steinhauer, S.A. Wharton, L.K. Tamm, Interaction of mutant influenza virus hemagglutinin fusion peptides with lipid bilayers: probing the role of hydrophobic residue size in the central region of the fusion peptide, Biochemistry 38 (1999) 15052–15059.
[41] B.R. Brooks, C.L. Brooks, A.D. Mackerell, L. Nilsson, R.J. Petrella, B. Roux, Y. Won, G. Archontis, C. Bartels, S. Boresch, A. Caflisch, L. Caves, Q. Cui, A.R. Dinner, M. Feig, S. Fischer, J. Gao, M. Hodoscek, W. Im, K. Kuczera, T. Lazaridis, J. Ma, V. Ovchinnikov, E. Paci, R.W. Pastor, C.B. Post, J.Z. Pu, M. Schaefer, B. Tidor, R.M. Venable, H.L. Woodcock, X. Wu, W. Yang, D.M. York, M. Karplus, CHARMM: the biomolecular simulation program, Journal of Computational Chemistry 30 (2009) 1545–1614.
[42] T.B. Woolf, B. Roux, Molecular dynamics simulation of the gramicidin a channel in a phospholipid bilayer, Proceedings of the National Academy of Sciences of the United States of America 91 (1994) 11631–11635.
[43] T.B. Woolf, B. Roux, Molecular dynamics simulation of the gramicidin a channel in a phospholipid bilayer, PROT: Struct Funct Genomics 24 (1996) 92–114.
[44] S. Berneche, M. Nina, B. Roux, Molecular dynamics of melittin in a dimyristoyl phosphatidylcholine bilayer membrane, Biophysical Journal 75 (1998) 1603–1618.
[45] S. Berneche, B. Roux, Molecular dynamics of the KcsA K+ channel in a bilayer membrane, Biophysical Journal 78 (2000) 2900–2917.
[46] W.L. Jorgensen, J. Chandrasekhar, J.D. Madura, R.W. Impey, M.L. Klein, Comparison of simple potential functions for simulating liquid water, The Journal of Chemical Physics 79 (1983) 926–935.
[47] E. Lindahl, B. Hess, D. van der Spoel, A package for molecular simulation and trajectory analysis, Journal of Molecular Modeling 7 (2001) 306–317.
[48] I. Chandrasekhar, M. Kastenholz, R.D. Lins, C. Oostenbrink, L.D. Schuler, D.P. Tieleman, W.F. van Gunsteren, A consistent potential energy parameter set for lipids: dipalmitoylphosphatidylcholine as a benchmark of the GROMOS96 45A3 force field, European Biophysics Journal 32 (2003) 67–77.
[49] H.J.C. Berendsen, J.R. Grigera, T.P. Straatsma, The missing term in effective pair potentials, The Journal of Physical Chemistry 91 (1987) 6269–6271.
[50] W.F. van Gunsteren, H.J.C. Berendsen, Gromos-87 Manual, 1987.
[51] S. Miyamoto, P.A. Kollman, SETTLE: an analytical version of the SHAKE and RATTLE algorithm for rigid water models, Journal of Computational Chemistry 13 (1992) 952–962.
[52] W. Kabsch, C. Sander, Dictionary of protein secondary structure: pattern recognition of hydrogen-bonded and geometrical features, Biopolymers 22 (1983) 2577–2637.
[53] J.F. Nagle, S. Tristram-Nagle, Lipid bilayer structure, Current Opinion in Structural Biology 10 (2000) 474–480.
[54] H.I. Petrache, S.W. Dodd, M.F. Brown, Area per lipid and acyl length distributions in fluid phosphatidylcholines determined by 2H NMR spectroscopy, Biophysical Journal 79 (2000) 3172–3192.
[55] D.P. Tieleman, L.R. Forrest, M.S.P. Sansom, H.J.C. Berendsen, Lipid properties and the orientation of aromatic residues in OmpF, influenza M2, and alamethicin systems: molecular dynamics simulations, Biochemistry 37 (1998) 17554–17561.